Nuclear Materials and Energy 33 (2022) 101263

Contents lists available at ScienceDirect

Nuclear Materials and Energy

journal homepage: www.elsevier.com/locate/nme

Effect of continuously flowing liquid Li limiter on particle and heat fluxes during H-mode discharges in EAST

G.Z. Zuo [a,*], C.L. Li [a,b], R. Maingi [c], X.C. Meng [a,d], D. Andruczyk [e], P.J. Sun [a], Z. Sun [a,c], W. Xu [a,d], M. Huang [a], Z.L. Tang [a], D.H. Zhang [a], Y.J. Chen [a], Q. Zang [a], Y.M. Wang [a], Y.F. Wang [a], K. Tritz [f], J.S. Hu [a,g,*]

[a] Institute of Plasma Physics, Chinese Academy of Sciences, Hefei, Anhui 230031, China
[b] University of Science and Technology of China, Hefei, Anhui 230026, China
[c] Princeton University Plasma Physics Laboratory Princeton, NJ 08543, USA
[d] Institute of Energy, Hefei Comprehensive National Science Center, Hefei 230031, China
[e] Center for Plasma Material Interactions, University of Illinois Urbana-Champaign, MD 21211, USA
[f] Johns Hopkins University, Baltimore, MD 21211, USA
[g] CAS key Laboratory of Photovoltaic and energy conservation materials, Hefei 230031, China

ARTICLE INFO

Keywords:
Liquid Li
Particle flux
Heat flux
H-mode
EAST

ABSTRACT

Particle and heat fluxes were successfully controlled by using a continuously flowing liquid Li (FLiLi) limiter in the H-mode discharges with high plasma heating power in the Experimental Advanced Superconducting Tokamak device. There were strong interactions between the FLiLi limiter and high-power plasma with a ~ 8.3 MW source heating power, and successively, a bright Li radiation ring was produced, which effectively decreased fuel particle recycling by approximately 50%. Due to Li efflux from FLiLi during a series of high-power discharges, an obvious real-time wall conditioning effect was produced, and fuel particle recycling further decreased. Moreover, the value of Z_{eff} decreased from 2.3 to 1.6 due to a decrease in impurity sources; this was attributed to the accumulation of Li deposited on the first wall, which effectively protected the wall materials. The decreased recycling and impurity radiation achieved high-energy confinement plasma, and the average stored energy increased up to ~ 290 kJ. Moreover, due to the effect of Li vapor shielding, nearly 30% plasma heat flux was dissipated before it arrived at the Li limiter. These results promote further exploration of liquid Li solutions for the critical challenge of heat flux handling and particle control in fusion power plants.

Introductions

Particle and power handling are among some of the major challenges for future fusion devices [1]. Liquid plasma-facing components (PFCs) have been proposed as an alternative to solid PFCs; it is expected that liquid metal wall can withstand the high particle and heat loads in fusion reactors of future [2,3]. The lifetime of liquid wall is less problematic because a liquid can replenish itself, which prevents damage accumulation, leading to a longer lifetime than solid PFCs. Furthermore, the particle and heat exhaust by adsorption effect, convective movement of the liquid metal, and vapor shielding are beneficial for the application of liquid PFCs in fusion reactors [4,5].

Most contemporary liquid metal research is focused on Li [6,7], Sn, and Li-Sn [8]. Studies on liquid Li have been successfully carried out in many tokamaks, such as T-11 M [5], T-15 [9], FTU [10], EAST[11], and in some laboratories. Different types of liquid Li walls, such as free surface, capillary porous surface [5], 3D printed structures, and trench structural designs, have been designed and tested. In all liquid Li discharges, lower recycling and impurity levels have been achieved, and it has been confirmed that the application of liquid Li PFCs can enhance plasma performance [12]. Moreover, liquid Li surface can withstand heat flux of > 10 MW/m^2 [17], partly due to heat load mitigation on the first wall via Li radiation. In the T-11 M tokamak, heat load mitigation on the first wall due to Li radiation has been observed, and the radiated power fraction reached up to 80% of the ohmic heating power [5]. At COMPASS [13,14], good exhaust capability was observed for liquid Li and Li-Sn for inter-edge localized mode (ELM) steady-state perpendicular heat fluxes of up to 12 MW/m^2, along with a local peak energy

* Corresponding authors.
E-mail address: zuoguizh@ipp.ac.cn (G.Z. Zuo), hujs@ipp.ac.cn (J.S. Hu).

https://doi.org/10.1016/j.nme.2022.101263
Received 15 June 2022; Received in revised form 26 August 2022; Accepted 22 September 2022
Available online 23 September 2022
2352-1791/© 2022 The Authors. Published by Elsevier Ltd. This is an open access article under the CC BY-NC-ND license (http://creativecommons.org/licenses/by-nc-nd/4.0/).

fluence at the module of order 15 kJ·m^{-2}. At Pilot-PSI [4], the incident heat flux decreased by approximately 30% compared to a solid Mo target due to the effect of liquid metal vapor shielding when subjected to an incident heat flux of 16 MW·m^{-2} over 20 s. The oscillation of liquid metal surface temperature induced by vapor shielding has also been investigated [15]. During vapor shielding, regular oscillations in surface temperature were observed at the Sn target. In Magnum-PSI, a liquid Li divertor target prototype with an internal reservoir pre-filled with Li was tested with power loads up to 9 ± 1 MW·m^2.

In HT-7, since 2009, various static and flowing liquid Li limiters have been designed and tested to master the key technologies of liquid Li wall application and improve plasma performance. Some exciting results have been obtained during liquid Li experiments, such as 20–30% reduction in particle recycling, 10–20% decrease in impurity emission, and 20% increase in energy confinement [16-18]. However, efflux of liquid Li from Li surface occurred, which was attributed to Li droplet ejection, probably due to surface oxidation [13], and the J × B electromagnetic force effect, which led to plasma disruption [19].

Based on the results of these studies, a slowly flowing liquid Li limiter (FLiLi), based on the concept of a thin flowing film, was selected for the EAST device. Three generations of FLiLi limiters have been developed and successfully tested in EAST since 2014 [20]. It has been confirmed that liquid Li can be driven by an innovative in-vessel DC electromagnetic J × B pump to form a recirculating loop. FLiLi design has been continuously upgraded, which has led to the improved liquid Li surface coverage (>80%), elimination of surface erosion, and higher heat exhaust capability [21]. Promising results have been obtained during FLiLi operations, including the reduction in impurities and recycling to improve plasma confinement, mitigation of plasma and Li wall interactions, and mitigation of ELM activity in H-mode plasmas during FLiLi operation, with up to approximately 4.5 MW auxiliary heating power [11]. Based on these efforts, remarkable engineering and physical advances of FLiLi wall have been made, and the improved particle and heat exhaust capacities have been verified at relatively low plasma heat power of ≤ 4.5 MW. Further investigations are required on particle and heat handling capacities with higher heating power.

This study presents some results of handling particle and heat fluxes during H-mode discharges with continuously a FLiLi limiter in the EAST device. Section 2 describes the experimental setup and related diagnostics. In Section 3, fuel and impurity particle control during H-mode plasma with auxiliary heating power up to 8.3 MW and heat flux estimation is demonstrated. Discussion and conclusion are presented in Section 4.

Experimental setup

As shown in Fig. 1, the FLiLi limiter system was installed at the H port in EAST, and it included a distributor, guide plate, collector, and two electromagnetic (EM) pumps. The FLiLi used TZM (Titanium-Zirconium-Molybdenum Alloy with > 99% Mo) as the substrate material, and its dimensions were 320 mm × 300 mm × 18 mm (length × height × depth). Eight heater cartridges inserted into internal grooves were used to adjust the temperature of the target plate. The vertical current of the EM pump resulting from the external voltage with the horizontal toroidal magnetic field of EAST led to a upward J × B bulk force on the liquid Li; thereafter, electromagnetically driven liquid Li flowed from the collector to the distributor, and then through the TZM target surface to the collector, completing a circle [19,20].

During the liquid Li experiment, the limiter was inserted into the vacuum chamber of EAST and baked at 300–400 °C for approximately 24 h to release impurity gases and enhance the wetting of liquid Li on the surface of TZM. The usual morning routine of pre-run Li wall coating was cancelled for a clearer comparison of plasma performance before and during FLiLi operation. The plasma discharges adopted an upper single null (USN) diverted configuration. During the liquid Li experiment, the position of the limiter was scanned for R values in the range

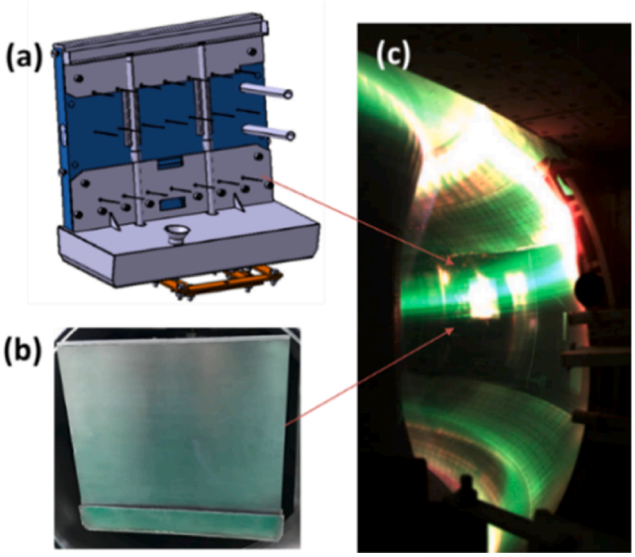

Fig. 1. FLiLi structure drawing: (a) back view of FLiLi, (b) front view of FLiLi, (c) photo of plasma discharge with FLiLi.

2.40–2.31 m (with the separatrix at R = ~2.295 m) to ensure a safe distance between the last closed field surface (LCFS) and the limiter to reduce the influence of liquid Li on core plasma. In addition, the auxiliary heating power (including electron cyclotron resonance heating (ECRH), lower hybrid wave (LHW), and neutral beam injection (NBI)) was scanned from 0 to approximately 8.3 MW.

IR and CCD cameras were used to measure the temperature of the limiter and monitor the condition of the PFC surface of the limiter during the FLiLi experiment. In addition, the thermocouples (TCs) embedded in the limiter plate collected temperature data during plasma discharge. Due to the low sampling rate of TCs, the IR camera was used to capture the temperature of liquid Li surface. The temperature from the IR camera was sensitive to the surface emissivity of liquid Li. To obtain more accurate emissivity, the surface emissivity of liquid Li was calibrated in each discharge by combining the data from the TCs and the IR camera.

Results

Fuel and impurity particle control during high-power plasma

Fig. 2 compares three typical shots with similar plasma current, density, and plasma configuration with Rsep. = 2.29 m at the FLiLi position. Shot 81510 was a reference shot without FLiLi operation, and shots 81637 and 81660 had the same EM-driven current and different FLiLi positions (limiter positions were R = 2.35 m and R = 2.36 m, respectively). Compared with the reference shot, the Li-II line emission intensity (emitted by Li^+ ions at 548.5 nm) was 1.4 and 2 times higher at these limiter positions, respectively. Inward movement of the FLiLi position led to obvious ~ 50% (R = 2.35 m) and ~ 90% (R = 2.36 m) decreases in the upper divertor Dα line emission intensity. Although shot 81660 had weak interaction between plasma and FLiLi, the effect of Li coating obviously led to a considerable reduction in recycling due to Li efflux from FLiLi and deposition via approximately 23 shots from shot 81637. With strong interaction between FLiLi and plasma (shot 81637), the average stored energy increased up to ~ 290 kJ with total source heating power of 8.3 MW using LHW, NBI, and ECRH, which was approximately 23 kJ higher than the reference shot; however, this was partly attributed to the slightly higher ECR heating power. Moreover, the stored energies during shot 81660 and reference shot were almost the same, and the LHW heating power was 500 kW lower during shot 81660 than that during the reference shot.

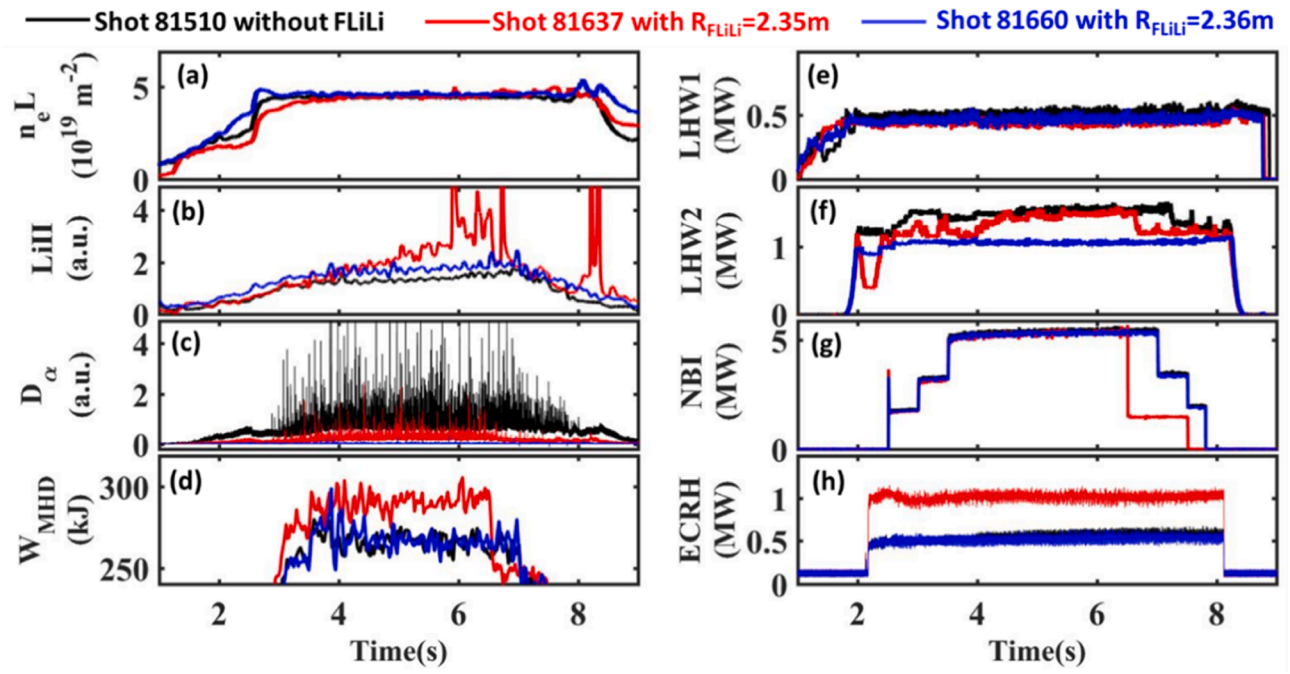

Fig. 2. Comparison of three typical plasmas with and without FLiLi (Ip = 0.55 MA; nel = ~4.3 × 10^{19} m^{-2}, USN, Rsep. = 2.28 m at FLiLi position; shot 81637 with limiter position R = 2.35 m, shot 81660 with limiter position R = 2.36 m). (a) Line-integrated electron density, (b) Li-II line emission intensity, (c) Dα line emission intensity from the upper divertor, (d) stored energy (Wdia), (e) LHW (2.45 GHz) heating power, (f) LHW (4.6 GHz) heating power, (g) total NBI heating power, and (h) ECRH heating power in the three shots.

Furthermore, gradual ELM mitigation during FLiLi operation was evident from the evolution of Dα emission. Compared to the ELM activity in shot 81510, the ELM frequency and amplitude both decreased, which is consistent with previous FLiLi results [22]. The ELM mitigation operation region was further extended to higher heating power, which is beneficial for mitigating transient high heat flux from ELM bursts in contemporary as well as future fusion devices.

In addition to recycling behaviors, the impurities also produced significant changes with and without the FLiLi limiter. Fig. 3 compares effective ion charge Z_{eff} representing the global impurity content during shots 81510, 81637, and 81660. Z_{eff} increased from approximately 1.7 to 2.3 during shot 81510 without FLiLi operation, indicating that the impurities were obviously accumulated. During shot 81637, which has a slightly higher heating power than shot 81510, Z_{eff} increased from approximately 1.9 to 2.3. The main impurities with FLiLi were Fe and Mo coming from the substrate and collector material of FLiLi due to strong interaction between the plasma and the limiter, which has been analyzed and presented in a previous study [22]. The value of Z_{eff} remained almost constant at approximately 1.6, and no obvious impurities accumulated during shot 81660. In addition to the reduced impurity sputtering resulting from the weaker interaction between plasma and limiter substrate due to farther limiter position from the plasma, the decreased impurity was probably attributed to the accumulation of Li resulting from Li evaporation, sputtering, and Li burst, which was deposited on the first wall to effectively protect the wall materials.

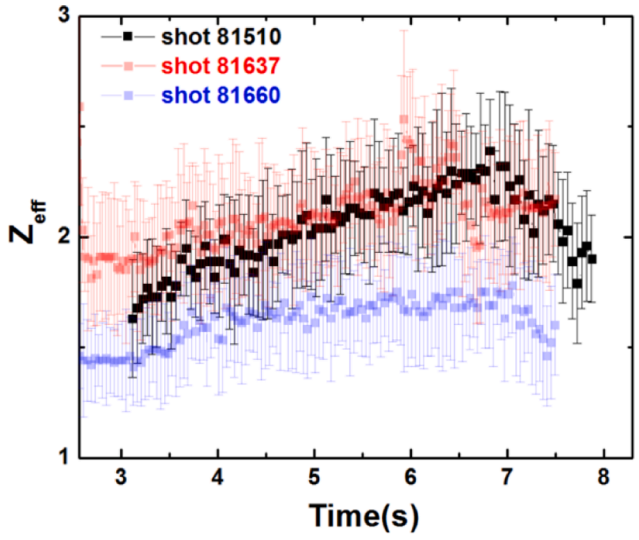

Fig. 3. Comparison of Z_{eff} during three typical shots with and without FLiLi. Black, red and blue lines represent Z_{eff} in shots 81510, 81637, and 81660, respectively. (For interpretation of the references to colour in this figure legend, the reader is referred to the web version of this article.)

Fig. 4 compares the plasma T_e measured by Thomson scattering (TS), n_e in core from the TS, and edge plasma density from the reflectometry profiles [23] at 5.11 s with and without FLiLi operation. The core T_e and n_e increased significantly, which were main contributions to 23 kJ higher plasma stored energy in Fig. 2. Furthermore, the edge plasma density with FLiLi was slightly lower than that without FLiLi. Due to FLiLi operation, fuel particle from plasma was captured by flowing liquid Li. Meanwhile, the Li coating layer from Li efflux from FLiLi owing to Li evaporation, sputtering, and Li burst could also capture fuel particles, which resulted in less fuel particles returning into edge plasma, thereby decreasing particle recycling. Accompanied by decreased fuel particle source at edge zone, less fuel particle ionization was produced and there was lesser contribution to edge plasma density. Decreased pedestal plasma density with similar plasma T_e produced a lower pedestal plasma pressure, which was helpful for decreasing pedestal pressure gradient and mitigating ELM [24]. These T_e and n_e profiles were consistent with mitigated ELM frequency and amplitude.

Heat flux estimation during H-mode plasma

To investigate the heat flux characteristics during H-mode plasma with type-I ELM, the radial location of the limiter was moved to R =

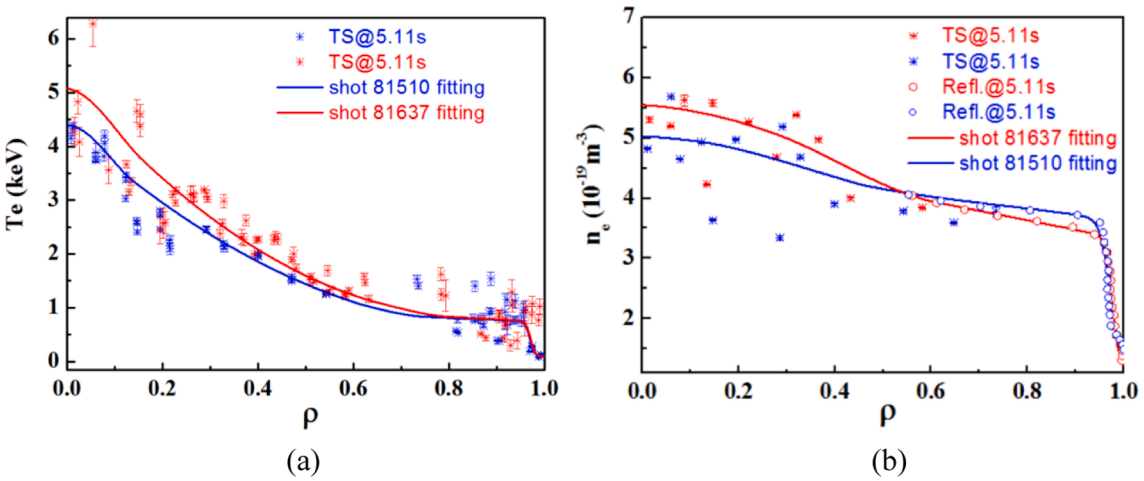

Fig. 4. Comparison of plasma T_e and n_e profiles with and without FLiLi operation: (a) T_e profiles from TS, (b) plasma density profiles from TS and the reflectometry.

~2.31 m; the total auxiliary heating source power was ~ 4.7 MW, with ~ 1.6 MW of LHW and 3.1 MW of NBI. The basic plasma parameters are shown in Fig. 5, with $n_e \sim 3.7 \times 10^{19}$ m^{-3}, $I_p = 450$ kA, in a USN configuration, and H-mode (type-I ELM) discharge with a low $q_{95} \sim 5.4$. The initial temperature of the limiter was ~ 450 °C, and the apparent red neutral Li vapor cloud at 0.22s is shown in Fig. 6(a) (as measured by a CCD camera, from port D in the toroidal direction away from liquid Li limiter). Li efflux and transport processes were apparent after 4.5 s, and the strong Li emission included both neutral Li atoms and ions filled in the scrape-off layer (SOL) region. From the CCD visible images, the plasma interaction was located mainly in the upper half of the limiter, and the peak temperature occurred at the right side of the limiter, as measured by the IR camera and TCs. During plasma discharge, the IR camera temperature measurements were saturated at some regions on the right side of the limiter surface; therefore, unsaturated positions were used for the Li surface heat flux analysis. Six IR temperature measurement positions on the limiter surface were selected, spanning from the distributer to the collector (Fig. 6(b)).

The temperature evolution at positions 3–6 is shown in Fig 7. The initial temperature of these positions was same at approximately 3 s. From ~ 3–4 s, the liquid Li surface temperature increased rapidly and Li line emission intensity was enhanced (Fig. 7 and Fig. 5(c), respectively) due to increased heating power. Furthermore, the temperature difference gradually increased from top to bottom. The maximum temperature was from the middle upper position (3), and the minimum temperature was at the bottom position (6). Moreover, the temperature change trends at different positions were consistent, and the rate of temperature increase slowed down. The heat flux on the limiter can be roughly estimated by a 1D heat flux calculation code. 1D heat conduction equation in a solid is given using equation (1).

$$k\frac{\partial T^2}{\partial^2 x} = \rho c \frac{\partial T}{\partial t} \tag{1}$$

where κ, ρ, and c represent the effective values of the TZM thermal conductivity, density, and heat capacity, respectively. The thickness of the TZM plate was 18 mm. The liquid lithium was very thin; therefore, the temperature at the top of the TZM plate was close to the surface temperature. T(x = 0) = Ts was the top layer condition on the TZM plate. At the bottom of the TZM plate, heat insulation was assumed, $\frac{\partial T}{\partial x}(x = 19mm) = 0$. Then, the heat flux at the top of the TZM was calculated with an implicit finite different method [25]. As shown in Fig. 7, the heat flux value decreased from ~ 1.72 MW to ~ 1.20 MW when the discharge time changed from ~ 4.5 s to ~ 6.5 s, which was attributed to the significant increase in Li emission intensity shown in Fig. 5(c); heat flux decreased by approximately 30% due to the effect of Li vapor.

At the beginning of the discharge, the plasma heat flux heated the liquid Li, rapidly increasing the surface temperature. When the Li surface temperature was > 550 °C, the Li evaporation rate was sufficiently high to form a Li vapor layer around the liquid Li limiter. The Li line emission from the Li vapor could dissipate significant energy from the plasma exhaust prior to its arrival at the liquid Li surface. Therefore, Li vapor could decrease the rate of temperature increase. In addition, significant temperature oscillations of the liquid Li surface were observed during H-mode plasma discharge with type-I ELM. The oscillation amplitude as well as frequency of the liquid Li surface temperature showed a strong correlation with the surface temperature of liquid Li. The temperature oscillations gradually enhanced when Li surface temperature was > 550 °C; this was because of the enhanced Li efflux mainly from Li evaporation. Temperature oscillation was thus an indispensable mechanism for the self-regulation of the heat flux dissipation by the liquid Li surface.

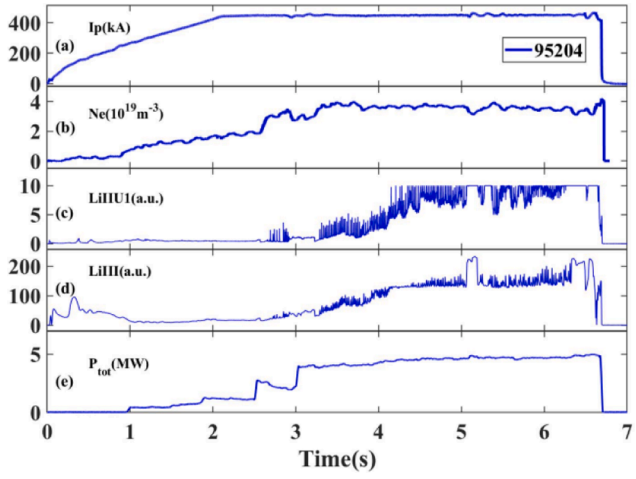

Fig. 5. Basic plasma parameters in shot 95204. (a) Plasma current, (b) line-averaged electron density, (c) Li-II emission intensity in upper divertor area, (d) LiIII line emission, and (e) total auxiliary heating power including, with 1.6 MW LHW and ~ 3.1 MW NBI.

Summary

Particle and heat flux control was achieved by using a FLiLi limiter during high-power H-mode discharges on the EAST device. The fuel recycling indicated by divertor Dα line emission intensity decreased by ~ 2 times with FLiLi operation compared with shots captured without

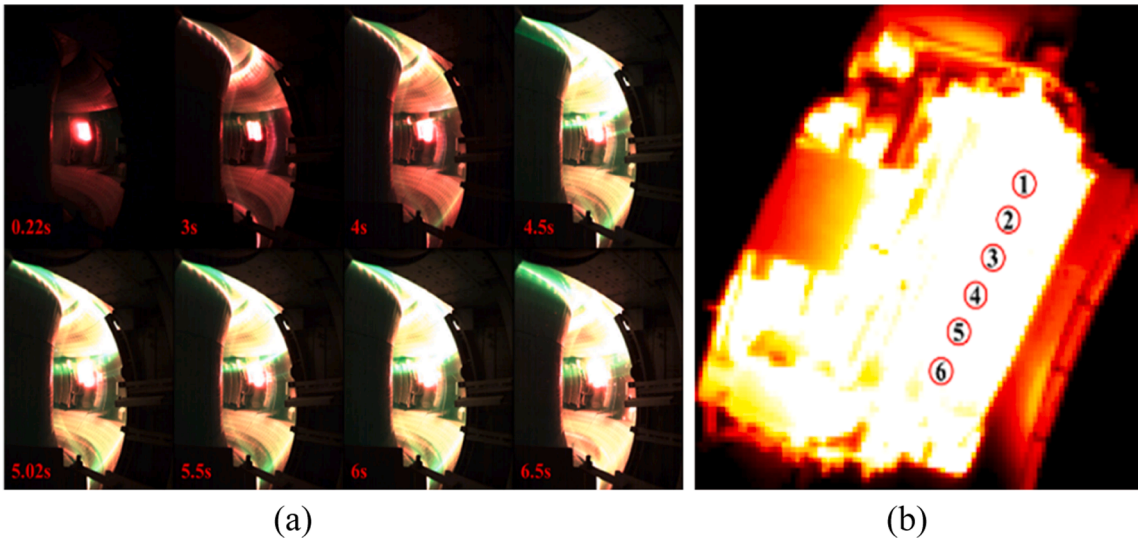

Fig. 6. (a) CCD camera images and (b) IR camera image in shot 95,204.

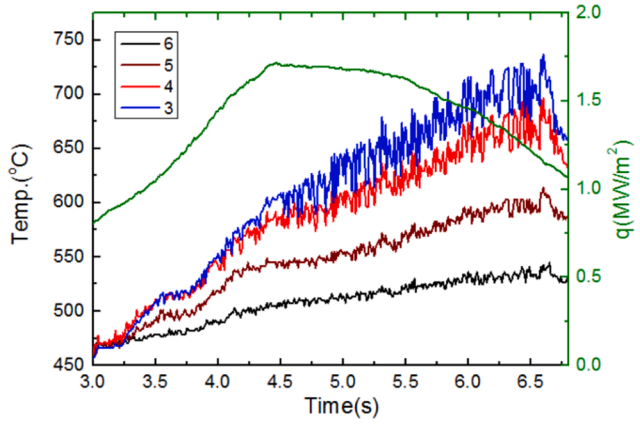

Fig. 7. Evolution of temperature and heat flux at different limiter positions as time during discharge.

the FLiLi limiter. Gradual ELM mitigation during FLiLi operation was evident, as estimated from the evolution of Dα emission. With a sequence of discharges with FLiLi operation, the value of Z_{eff} decreased from 2.3 to ~ 1.6. A high stored energy plasma up to ~ 290 kJ with approximately 8.3 MW source plasma heating power was successfully obtained due to the improved particle control capability by using liquid Li. Moreover, plasma heat flux mitigation by the Li vapor shielding effect was also observed, and ~ 30% plasma heat flux was dissipated prior to its arrival at the liquid Li surface owing to the Li vapor shielding effect. These results show that liquid Li as PFCs have promising applications for achieving steady-state high parameter plasmas with strong particle and heat exhaust capacities, making it a critical research topic for future fusion devices.

As a next step, we aim to develop several diagnostic systems on the FLiLi limiter, such as probes for measuring plasma temperature and density near liquid Li surface, laser-induced breakdown spectroscopy for measuring liquid Li thickness and velocity, and a new type of liquid Li limiter with a 3D-printed W substrate.

CRediT authorship contribution statement

G.Z. Zuo: Conceptualization, Data curation, Writing – original draft. **C.L. Li:** Methodology, Software. **R. Maingi:** Supervision, Funding acquisition. **X.C. Meng:** Visualization, Investigation. **D. Andruczyk:** Supervision, Funding acquisition. **P.J. Sun:** Resources. **Z. Sun:** Visualization, Investigation. **W. Xu:** Visualization, Investigation. **M. Huang:** Visualization, Investigation. **Z.L. Tang:** Visualization, Investigation. **D. H. Zhang:** Visualization, Investigation. **Y.J. Chen:** Resources. **Q. Zang:** Resources. **Y.M. Wang:** Resources. **Y.F. Wang:** Resources. **J.S. Hu:** Supervision, Funding acquisition.

Declaration of Competing Interest

The authors declare that they have no known competing financial interests or personal relationships that could have appeared to influence the work reported in this paper.

Acknowledgement:

This research is funded by the National Key Research and Development Program of China (2017YFE0301100, 2022YFE03130000), National Nature Science Foundation of China (11905138, 11905148, 11905254), the U.S. Dept. of Energy contract DE-AC02-09CH11466 and grant DE-SC0016553, Users with Excellence Program of Hefei Science Center CAS (2020HSC-UE010), and Interdisciplinary and Collaborative Teams of CAS.

References

[1] S. Brezinsek, et al., Nucl. Fusion 57 (2017), 116041.
[2] R.J. Goldston, et al., Nucl. Mater. Energ. 12 (2017) 1118.
[3] E.D. Emdee, et al., Nucl. Mater. Energ. 19 (2019) 244.
[4] G.G. van Eden, et al., Phys. Rev. Lett. 116 (2016), 135002.
[5] S.V. Mirnov, et al., Plasma Phys. Control. Fusion 48 (2006) 821.
[6] V.A. Krupin, et al., Plasma Phys. Control. Fusion 62 (2020), 025019.
[7] P. Rindt, et al., Nucl. Fusion 58 (2018), 104002.
[8] F.L. Tabares, et al., Nucl. Mater. Energ. 12 (2017) 1368.
[9] J.N. Brooks, et al., J. Nucl. Mater. 290 (2001) 185.
[10] G. Mazzitelli, et al., Fusion eng. design 86 (2011) 580.
[11] G.Z. Zuo, et al., Nucl. Fusion 59 (2019), 016009.
[12] R. Majeski, et al., Phys. Rev. Lett. 97 (2006), 075002.
[13] J. Horacek, et al., Nucl. Mater. Energ. 25 (2020), 100860.
[14] R. Dejarnac, et al., Nucl. Mater. Energ. 25 (2020), 100801.
[15] G.G. van Eden, et al., Nat. Commun. 8 (2017) 192.
[16] G.Z. Zuo, et al., J. Nucl. Mater. 438 (2013) S90.
[17] G.Z. Zuo, et al., J. Nucl. Mater. 415 (2011) S1062.
[18] J. Ren, et al., Phys. Scr. T159 014033 (5 (2014) pp).
[19] G.Z. Zuo, et al., Fusion Eng. Des. 89 (2014) 2845.
[20] J.S. Hu, et al., Nucl. Fusion 56 (2016), 046011.
[21] G.Z. Zuo, et al., Rev. Sci. Instrum. 88 (2017), 123506.
[22] G.Z. Zuo, et al., Phys. Plasmas 27 (2020), 052506.

[23] X. Zhu, et al., Fusion Eng. Des. 131 (2018) 29.
[24] R. Maingi, et al., Nucl. Fusion 52 (2012), 083001.
[25] K.F. Gan, et al., J. Nucl. Mater. 438 (2013) S364.